Available online at www.sciencedirect.com
SCIENCE DIRECT®
International Journal of Mass Spectrometry 227 (2003) 289–302
International Journal of Mass Spectrometry
www.elsevier.com/locate/ijms

Review

Guided ion beam studies of transition metal–ligand thermochemistry

P.B. Armentrout*

Department of Chemistry, University of Utah, Salt Lake City, UT 84112, USA

Received 14 May 2002; accepted 15 October 2002

Abstract

Studies of organometallic chemistry in the gas phase can provide substantial quantitative information regarding the interactions of transition metals with a wide variety of covalently and noncovalently bound ligands. In this review, the technique of guided ion beam tandem mass spectrometry for the measurement of thermodynamic information is highlighted. Periodic trends in covalent bonds between first, second, and a few third row transition metals and small ligands are discussed. Periodic trends in covalent versus noncovalent metal ligand bonds are compared and fluctuations in sequential noncovalent bonds (solvation) as a function of different metals are reviewed. In all cases, electronic effects that can be used to understand the various trends are elucidated. Finally, recent results for ligands covalently bound to metal clusters are reviewed.

Keywords: Bond energies; Clusters; Covalent bonds; Guided ion beam; Noncovalent bonds; Thermochemistry; Transition metal ions

1. Introduction

Stable 18-electron complexes are the starting materials in organometallic reactions and homogeneous catalysis, but the key reactive intermediates are coordinatively unsaturated transition metal–ligand complexes that have an open site of reactivity on the metal center formed by loss of one or more ligands from the stable reagent. These unsaturated intermediates are good catalysts precisely because they are reactive, but this also makes them transient and difficult to study. Therefore, little is known about the thermodynamics of such reactive species, even though such information would enable predictions of the feasibility of desired reaction schemes. Likewise, the key intermediates in heterogeneous catalysis are molecular fragments bound to the surface. Although techniques are readily available to measure bond energies of intact molecules (e.g., CO, NH_3, C_2H_4) and atoms bound to surfaces, data for molecular fragments bound to surfaces is nearly absent. Although gas-phase chemistry cannot possibly characterize the bond energies of all ligands with all metals, metal complexes, and metal surfaces, it can provide a quantitative measure of the strength of typical interactions and the effects of adjoining ligands (including other metals) on these interactions.

Among the techniques available for measuring thermodynamics of gas-phase species is guided ion beam

* Tel.: +1-801-581-7885; fax: +1-801-581-8433.
E-mail address: armentrout@chemistry.utah.edu (P.B. Armentrout).

1387-3806/03/$ – see front matter
doi:10.1016/S1387-3806(03)00087-3

mass spectrometry. This method examines reactions at hyperthermal energies, thereby allowing endothermic reactions to be studied. (The energy range accessible in guided ion beam instruments extends from energies as low as thermal, $3k_BT/2$ (300 K) = 0.03 eV = 3 kJ mol^{-1}, to hundreds of volts, 100 eV = $3k_BT/2$ at 750,000 K.) Analysis of the kinetic energy dependence of such reactions permits a measurement of the energy onset, which can be related to specific bond energies made or broken in the reaction. We have applied this methodology to a wide number of systems in order to measure periodic trends in transition metal ligand bond energies. Work on first row transition metals has been reviewed previously [1–4], including a systematic reevaluation of all previous work in our laboratory by Armentrout and Kickel [4]. These data, along with thermodynamic information from other laboratories, have been tabulated by Freiser [5]. Reasonably complete information from our laboratory for carbon ligands to second row transition metal ions has also been compiled and reviewed [6]. Recent progress has involved extensions to third row transition metal elements and expansion of the set of ligands considered, and evaluations of metal cluster–ligand bond energies. These advances are highlighted in the present work.

In many of our studies, the schematic reaction (1) is used to determine the thermochemistry of M^+–L bond energies.

$$M^+ + RL \rightarrow ML^+ + R \quad (1)$$

A simple example is formation of metal-methyl cations from ethane (L = R = CH_3). A slightly more complex case is the generation of methyl-methylidene cations (L = CH_2) which can be formed from methane (R = H_2), cyclopropane (R = C_2H_4), or ethylene oxide (R = CH_2O). Thermochemistry for neutral species can be determined in a related fashion by examination of reaction (2).

$$M^+ + RL \rightarrow ML + R^+ \quad (2)$$

Here the species R is chosen to have a low ionization energy (IE), such that reaction (2) competes effectively with reaction (1). Examples include formation of metal-hydrides from any number of hydride donors [R = $C(CH_3)_3$, CH_2NH_2], metal-methyls from *neo*-pentane [R = $C(CH_3)_3$], and metal oxides from NO_2 [L = O, R = NO]. Another very powerful type of reaction that we have used to derive thermodynamic data is collision-induced dissociation (CID), process (3) where Rg is an inert collision gas. We usually use Xe as Rg for reasons described elsewhere [7–9].

$$ML^+ + Rg \rightarrow M^+ + L + Rg \quad (3)$$

2. Experimental method

The guided ion beam mass spectrometers used in our laboratories [8,10,11] incorporate an ion source, a mass spectrometer used to select the ionic reactant, a reaction zone, a second mass spectrometer to analyze ionic products, and an ion detector. The key property of the various ion sources we use is the ability to generate ions having a characterized internal energy distribution. In the reaction zone, ion–neutral collisions occur over a well-defined path length at a pressure sufficiently low that products are usually the result of single collisions. The reaction zone also incorporates an octopole ion beam guide [12,13] comprising eight rods that symmetrically encircle the path of the ion beam. Opposite phases of radio frequency (rf) electric potentials are applied to alternate rods to create a potential well in the radial direction, perpendicular to the beam path. This potential well confines product ions and scattered reactant ions until they drift from the reaction region at which point they are accelerated, mass analyzed with a quadrupole mass filter, and detected. The use of an octopole field is preferred in such experiments as it perturbs the kinetic energy distribution of the ions less than the more common quadrupole field. The trapping potential greatly enhances the sensitivity of the experiment, permits routine examination of energies as low as thermal, and allows a straightforward measurement of the distribution and absolute zero of the ion kinetic energy. The detector is capable of detecting individual ions with near 100% efficiency. The raw experimental data, ion intensities as a function of ion kinetic energy, are converted to absolute reaction cross-sections as a function of energy in the center-of-mass frame as detailed previously [10].

3. Data analysis

As noted above, thermochemistry for metal–ligand bonds can be obtained from the thresholds, E_0, for endothermic reactions (1)–(3). For these processes, the reaction thresholds are related to the desired bond energies by Eqs. (4)–(6), respectively.

$$D_0(M^+–L) = D_0(R–L) - E_0(1) \quad (4)$$

$$D_0(M–L) = D_0(R–L) + IE(R) - IE(M) - E_0(2) \quad (5)$$

$$D_0(M^+–L) = E_0(3) \quad (6)$$

Threshold energies are determined by detailed modeling of the experimental cross-sections using a mathematical expression justified by theory [14,15] and experiment [16–22], Eq. (7).

$$\sigma(E) = \sigma_0 \sum g_i \frac{(E + E_i - E_0)^n}{E} \quad (7)$$

Here, σ_0 is a scaling factor, E the relative kinetic energy, and n an adjustable parameter. The sum is over the contributions of individual reactant states (vibrational, rotational, and electronic), denoted by i, with energies E_i and populations g_i ($\sum g_i = 1$). This expression assumes that all of the energy of the reactants (internal and translational) is available to the reaction and that the reaction efficiency and energy dependence (as determined by σ_0 and n, respectively) do not vary with the state i, which can be inaccurate for different electronic states.

Before comparison with the experimental data, the model of Eq. (7) is convoluted over the explicit distributions of the kinetic energy of the neutral and ion reactants, as described previously [10,23,24]. The σ_0, n, and E_0 parameters are then optimized by using a least squares analysis to give the best reproduction of the data. Because Eq. (7) includes all sources of energy for the reactants, the thresholds and bond energies obtained using these methods correspond to 0 K thermochemistry. Uncertainties in E_0 reflect the range of threshold values obtained for different data sets with different values of n and the error in the absolute energy scale. In cases where the internal energy of the reactants is appreciable and the vibrational frequencies are not well established, the uncertainty also includes variations in the calculated internal energy distribution of the reactants, E_i. The accuracy of the thermochemistry obtained by this modeling procedure is dependent on a variety of experimental parameters that have undergone extensive discussion [1,4,21].

To obtain accurate thermochemistry using Eqs. (4)–(6), it is assumed that the reactions have no barriers in excess of the endothermicities of the reactions studied. In contrast to many condensed phase reactions, the assumption of no reverse activation barriers is generally a reasonable one for gas-phase ion–molecule reactions because of the strong long-range ion–neutral interaction potential [25]. This is conclusively demonstrated by the common observation that exothermic ion–molecule reactions often proceed without an activation energy [22]. This assumption has been explicitly tested by comparing our results to systems where the thermochemistry is well established [17–21,26–30], although good sensitivity may be required to observe the true thermodynamic threshold in some cases [26]. Spin or orbital angular momentum conservation restrictions can lead to exceptional behavior [21,31] as can the presence of a tight-transition state (TS) along the reaction coordinate [32–35]. For CID reactions of organometallic complexes, quantum mechanics demonstrates that there should be no reverse activation energies, a consequence of the heterolytic bond cleavages involved [36], although dissociation to an excited state asymptote can occur [37].

Another important issue to address in threshold studies, particularly for CID processes, is to analyze only reactions involving single collisions between the ions and the neutral reactants. Multiple collisions lead to an ill-defined energy available to the reaction system. Rigorously single collision conditions are not achievable experimentally, but data for such conditions can be easily acquired by examining the dependence of the reaction cross-sections on the neutral reactant pressure and extrapolating the data to zero neutral pressure [37,38].

As the systems increase in size, the extraction of accurate thermodynamic thresholds requires consideration of the lifetime of the transient intermediates formed during reaction. When this lifetime becomes comparable to the time it takes ions to travel from the reaction region to the detector ($\sim 10^{-4}$ s), the threshold for reaction is observed to shift to higher energies, a "kinetic shift". We account for this effect by using RRKM (Rice–Ramsperger–Kassel–Marcus) theory [39] to calculate a dissociation probability as a function of the ion internal energy [40,41]. Characterization of the appropriate transition state becomes one of the limitations in such studies [42,43], although we have shown that a loose orbiting transition state (also called the phase space limit) is appropriate for many CID processes [41].

4. Bond energy bond order correlations

Metal–ligand (M^+–L) bond energies for first, second, and several third row transition metal cations with H, CH_3, CH_2, CH, O, and S are given in Table 1. Comparison of the latter two ligands has recently been reviewed [44]. These bond energies are determined using reaction 1 with the most common reagents being RL = H_2; C_2H_6 and CH_4; CH_4, c-C_3H_6, and c-C_2H_4O; CH_4; O_2 and CO; and COS and CS_2, respectively. Trends in these bond energies can be examined in several different ways.

One useful way of ascertaining the relative bond order of the metal ligand bonds is to compare with known organic and inorganic analogues, the L–L bond energies [45]. Such a bond energy bond order (BEBO) correlation plot is shown in Fig. 1 for the group 10 metals [4,46–51]. Clearly, for a specific metal, M^+–CH bonds are stronger than M^+–CH_2 bonds, which are stronger than M^+–CH_3 bonds. The latter are comparable to M^+–H bonds. This simply reflects the triple, double, and single bond character of these bonds as shown by how well the values track with the analogous organic L–L bond energies.

In the case of the Pt^+–CH bond energy, two values are shown in Fig. 1. The lower value (listed in Table 1) is the adiabatic bond energy, whereas the higher value has been adjusted by the average energy difference between the $Pt^+(^2D,5d^9)$ ground state and the $Pt^+(^4F,6s^15d^8)$ first excited state, 73 kJ mol^{-1} [52]. This reflects the fact that diabatic cleavage of the Pt^+–CH triple bond would form $Pt^+(^4F) + CH(^4\Sigma)$.

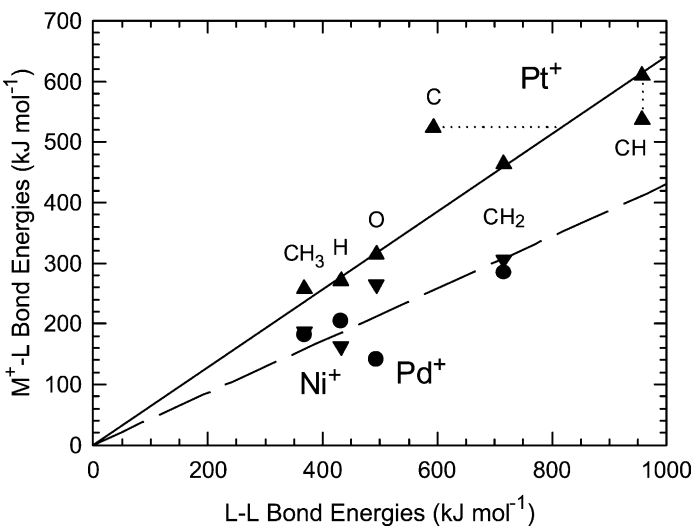

Fig. 1. Bond energies (in kJ mol^{-1}) for Ni^+ (closed inverted triangles), Pd^+ (closed circles), and Pt^+ (closed triangles) covalently bound to several ligands, L = CH_3, H, O, C, CH_2, and CH, vs. bond energies (in kJ mol^{-1}) of L–L. Lines are a guide to the eye.

Table 1
Covalent transition metal–ligand bond energies (0 K) in kJ mol^{-1}[a]

M	M^+–H	M^+–CH_3	M^+–CH_2	M^+–CH	M^+–O	M^+–S[b]
Sc	235(9)	233(10)	402(23)		689(6)	480(5)[c]
Ti	223(11)	214(3)	380(9)	478(5)	664(7)	457(7)[c]
V	198(6)	193(7)	325(6)	470(5)	564(15)	365(10)[d]
Cr	132(9)	110(4)	217(4)	294(29)	359(12)	259(16)[e]
Mn	199(14)	205(4)	286(9)		285(13)	243(23)[e]
Fe	204(6)	229(5)	341(4)	423(29)[f]	335(6)	297(4)[g]
Co	191(6)	203(4)	317(5)	420(37)[f]	314(5)	285(9)[h]
Ni	162(8)	187(6)	306(4)		264(5)	237(4)[i]
Cu	88(13)	111(7)	256(5)		130(12)[j]	200(14)[i]
Zn	228(13)	280(7)			161(5)	198(12)[i]
Y	256(8)[k]	236(5)	388(13)		699(17)[m]	530(8)
Zr	218(8)[k]	230(15)[l]	447(4)[l]	575(20)[l]	749(11)[m]	533(21)
Nb	220(7)[k]	199(11)[n]	428(9)[n]	581(19)[n]	688(11)[m]	532(10)
Mo	166(6)[k]	157(12)[l]	329(12)[l]	509(10)[l]	488(2)[m]	355(5)
Ru	156(5)[o]	160(6)[p]	344(5)[p]	502(12)[p]	368(5)[q]	288(6)
Rh	161(4)[o]	142(6)[r]	356(8)[r]	444(12)[r]	291(6)[q]	226(13)
Pd	200(4)[o]	181(10)[s]	285(5)[s]		141(11)[q]	197(6)
Ag	40(6)[o]	67(5)[t]	>107(4)[t]		119(5)[q]	123(13)
La	239(9)	217(15)	401(7)			
Lu	204(15)	176(20)	>230(6)			
Ta	219(5)[u]	196(3)[l]	>454[l]	575(9)[l]		
W	230(6)[u]	166(27)[l]	458(6)[l]	595(30)[l]		
Pt	271(5)[v]	258(8)[w]	463(3)[w]	536(10)[w]	315(5)[x]	

[a] Values are taken from [4] unless otherwise noted.
[b] Values are from [44] unless otherwise noted.
[c] [112].
[d] [113].
[e] [114].
[f] [115].
[g] [116].
[h] [117].
[i] [118].
[j] [119].
[k] [120].
[l] Preliminary values not yet thoroughly evaluated from work in progress.
[m] [121].
[n] [122].
[o] [48].
[p] [123].
[q] [47].
[r] [124].
[s] [46].
[t] [125].
[u] [126].
[v] [50].
[w] [49].
[x] [51].

The CH($^4\Sigma$) state is also an excited state (the ground state is $^2\Pi$) but the effects of this excitation energy are already included in the HC≡CH bond energy.

The value of the Pt^+–C bond energy is also interesting. Clearly, this bond energy does not fit the correlation with the C–C bond energy. This is simply explained by noting that Pt^+ has occupied 5dπ orbitals that can donate into the empty 2pπ orbital on C. Thus, PtC^+ has a covalent double bond augmented by a two-electron dative bond, making it stronger than Pt^+–CH_2. In that regard, it is closer to a triple bond, consistent with the observation that $D_0(Pt^+–C) \approx D_0(Pt^+–CH)$. In contrast, the PtO^+ bond energy is much weaker than that for PtC^+ and correlates nicely with the O_2 bond energy (Fig. 1). This is consistent with the fact that both PtO^+ ($^2\Pi$) and O_2 ($^3\Sigma_u^-$) molecules have electrons in π* antibonding orbitals (3 and 2, respectively), weakening the π-bonds.

Clearly, the covalent bonds to the first and second row metals are weaker than to the third row metal, differences that can be understood qualitatively on the basis of sd hybridization. sd hybridization is required to form multiple bonds (see above) and can enhance single bond formation if the sizes of the s and d orbitals are comparable. Energetically sd hybridization for the group 10 metals requires mixing metal ions in the ^{2}D ground state having a s^0d^9 configuration with those in the ^{4}F excited state having a s^1d^8 configuration. For Ni^+, the $^2D(4s^03d^9) \rightarrow {}^4F(4s^13d^8)$ promotion energy is 105 kJ mol^{-1}, but here spin-orbit interactions are weak such that the appropriate promotion energy to consider is probably $^2D(4s^03d^9) \rightarrow {}^2F(4s^13d^8)$, which is 162 kJ mol^{-1} [52]. For Pd^+, such hybridization is inefficient because the $^2D(5s^04d^9) \rightarrow {}^4F(5s^14d^8)$ promotion energy is very high, 308 kJ mol^{-1}. In the platinum system, the $^2D(6s^05d^9) \rightarrow {}^4F(6s^15d^8)$ promotion energy is only 73 kJ mol^{-1}, largely because of relativistic effects, which also help make the sizes of the 6s and 5d orbitals comparable [53,54], such that sd hybridization is efficient and energetically accessible.

These promotion energies help explain why no values for Ni^+–CH and Pd^+–CH have yet been measured. Here the promotion energy from the ^{2}D ground states to the appropriate s^1d^8 excited state are 162 and 308 kJ mol^{-1} [52], respectively, such that the correlation of Fig. 1 predicts that these bond energies should be roughly 250 and 100 kJ mol^{-1}, respectively. Apparently, these values are sufficiently weak that these species have not been observed as yet in the reactions of Ni^+ and Pd^+ with small alkanes. These promotion energies also explain the trends in the metals oxides, which at first glance appear anomalous given than $D_0(Ni^+–O)$ is substantially greater than $D_0(Pd^+–O)$. However, if the bonding is viewed as that between $M^+(s^1d^8)$ and $O(2p^4)$, then the bond energies correlate with the promotion energies noted above.

5. Periodic trends in metal–ligand bond energies

Fig. 2 shows bond energies to OH_x (x = 0–2) for the first row transition metal cations [4,55,56]. The double-humped trend observed is common to many transition metal properties and is found for both covalently bound ligands (OH and O) and noncovalent interactions (H_2O). Note however that the dip in the middle of the row changes for each ligand (i.e., it is at Mn^+ for H_2O and O and at Cr^+ for OH). These variations are easily rationalized. Consider first the formation of a single covalent bond between the metal ion and OH, which requires decoupling the electron on the metal used for bonding from the remaining nonbonding metal electrons. Because of the stability of the half-filled shell of ground state Cr^+(^{6}S, $4s^03d^5$), the energetic costs of this decoupling are relatively large and hence, the Cr^+–OH bond energy is a local minimum. For single covalent bonds to H and CH_3, this decoupling energy explains the variations in the bond energies quantitatively, as has been shown previously [4,57,58]. These correlations indicate that there is considerable s character in these covalent single bonds to the first row transition metal cations and find an “intrinsic” metal–ligand single bond energy (i.e., the bond energy expected for a metal prepared to bond strongly to a hydrogen atom or methyl group) of about 240 kJ mol^{-1} [4]. However, because the OH

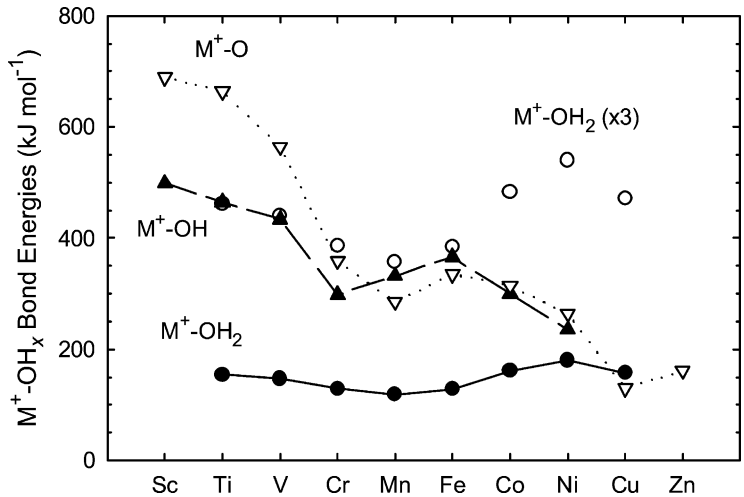

Fig. 2. Periodic trends in the bond energies (in kJ mol^{-1}) of first row transition metal cations with O (open inverted triangles), OH (closed triangles), and H_2O (closed circles; multiplied by 3, open circles).

group has two lone pair electrons, it can also form bonds with transition metals by π-backdonation to the metal. Clearly, this is most effective when the 3dπ orbitals are empty, which occurs to the left side of Cr. This explains why the Sc^+, Ti^+, and V^+ bonds to OH are much stronger than the later metals, on average by 120 ± 25 kJ mol^{-1} for each of two full dative bonds [4]. This effectively forms a triple bond, consistent with results from theory on $ScOH^+$, which shows that this species has a linear geometry [59]. For Mn^+, Fe^+, and Co^+, the enhancement associated with the dative bonds is approximately half this amount because the 3dπ orbitals are half-filled. The Ni^+–OH bond is particularly weak because it can only form one such half-dative π-bond. The stability of the $Cu^+(^1S, 3d^{10})$ filled shell configuration makes covalent bond formation with Cu^+ energetically costly. Apparently, the Cu^+–OH bond is sufficiently weak that it is difficult to measure.

For the metal-oxide cations, similar considerations hold. The early metal ions bind very strongly because the covalent double bond is augmented by a dative bond resulting from O(2p) donation into empty M(3d) orbitals. Here, the minimum bond energy occurs at Mn^+ because two electrons on the metal must be decoupled from the nonbonding electrons in order to make the covalent double bond with O. For the late metals, there is no augmentation of the bond energy from dative interactions, thus, the covalent M^+–O double bond is comparable to that for the covalent single bond + two half-dative bonds found for M^+–OH (Fig. 2).

Bond energies between M^+ and water are also shown in Fig. 2 [56]. Here there can be no covalent bonding character as the water ligand is closed shell, hence the variations in the bond energies are not as pronounced as for the covalently bound ligands. However, the bonding interaction is appreciable as a result of strong electrostatic and dative bonding interactions. If these bonds were purely electrostatic (i.e., involving only ion–dipole and ion–induced dipole interactions), then the variations in the bond energies across the periodic table would be even less pronounced than observed. The H_2O bond to Mn^+ is the weakest bond because the $^7S(4s^13d^5)$ ground state has no empty orbitals to accept electron density. Similarly, the bond to Fe^+ is weak because it also has an occupied 4s orbital in its $^6D(4s^13d^6)$ ground state and Cr^+ binds weakly because of its stable half-filled 3d shell. Overall, the bond energies observed here correspond to single dative bonds that are somewhat weaker than a covalent single bond. However, the bonds to the early metal

ions are augmented by π-donation from the ligand to the metal ion, for the same reasons discussed above. This trend is apparent when the M^+–OH_2 bond energies are compared with other ligands that either do not π-bond (such as NH_3) or where the ligands are π-acceptors (such as CO) [60].

6. Metal ion solvation: sequential dative metal–ligand bonds

In addition to metal–ligand bonds where there is only one ligand present, which now includes such complicated ligands as pyridine [61], pyrimidine [62], and adenine [63], guided ion beam methods have also been used to examine the solvation of transition metal cations by several ligands. These include all of the first row transition metal ions with ligands such as water [56], ammonia [60], and carbon monoxide [37,40,64–69], along with larger hydrocarbons: ethene [70] and benzene [71]. For selected metal ions, solvation by N_2 [66,72], NO [66,73], alkanes [74,75], formaldehyde [72], acetonitrile [76], acetone [77], dimethyl ether [78], and dimethoxyethane [79] have also been studied. The periodic variations in the first row transition metal carbonyl cations have been reviewed thoroughly [80] and trends in several of the other ligands have also been collected and examined [4,6,60,81]. Rather than repeating these collections, this article will illustrate some of the key considerations in understanding the trends observed for sequential ligation.

Fig. 3 shows the variations in dative bond energies for water bound to Na^+(^{1}S, $3s^0$) [29], Ni^+(^{2}D, $4s^0$, $3d^9$), and Cu^+(^{1}S, $4s^0 3d^{10}$) [56] metal ions. In comparing these systems, realize that Na^+ and Cu^+ have very similar ionic radii (0.98 and 0.96 Å, respectively [82]) and both have ^{1}S ground states, such that electrostatic interactions of ligands with these metal ions should be very similar. Although this expectation is realized for the third and fourth ligands ($x = 3$ and 4), the first two ligands differ dramatically in their bond energies to these two metal ions. Interestingly, the trends in these bond energies can be explained by returning to the concept of sd hybridization. The trend in the sequential bond energies of $Na^+(H_2O)_x$ are as expected for simple electrostatic bonds (i.e., they decrease monotonically), reflecting increasing ligand–ligand repulsion and decreasing electron

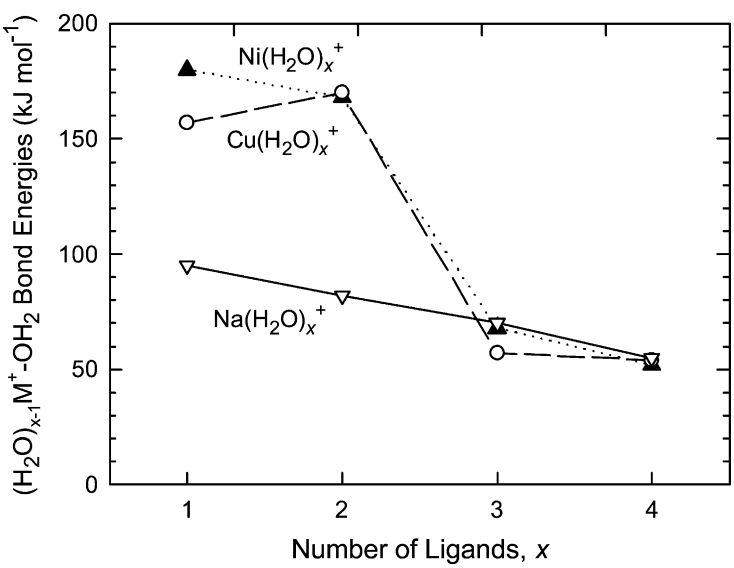

Fig. 3. Sequential bond energies (in kJ mol^{-1}) for water bound to Ni^+ (closed triangles), Cu^+ (open circles), and Na^+ (open inverted triangles).

deficiency at the metal center as a consequence of the electron donation from the ligands. For $Cu^+(H_2O)$, the empty 4s orbital and the doubly-occupied 3dσ orbital (which is aligned towards the ligand) hybridize with one another to form a $4s+3d\sigma$ hybrid with large lobes along the Cu–O internuclear axis and a $4s-3d\sigma$ hybrid with large lobes directed perpendicular to the Cu–O internuclear axis [83–85]. Two electrons are placed in the $4s-3d\sigma$ hybrid, leaving the $4s+3d\sigma$ hybrid empty and available to accept electron density from the water ligand. Because electron density has been removed from the metal–ligand axis, the ligand sees a higher effective nuclear charge, leading to a stronger bonding interaction. Because of the symmetry of the sd hybrids, two ligands located on opposite sides of the metal ion benefit from the hybridization, explaining why the first and second bonds to Cu^+ are strong. Indeed, the second bond energy is stronger than the first because the energetic cost of the hybridization is spread over two bond energies rather than just one. However, the third ligand is forced to interact with the electrons in the $4s-3d\sigma$ hybrid, leading to a sharp decline in the bond energies. In essence, the sd hybridization is no longer advantageous and the bond energies for $x = 3$ and 4 return to values similar to Na^+. $Ni^+(H_2O)_x$ shows a similar bonding pattern to $Cu^+(H_2O)_x$ except for the first ligand, which forms a stronger bond with Ni^+ because the 3dσ orbital is only singly occupied.

Although the information is less extensive, similar observations have been made for second and third row metal ions. For example, $Cu^+(CO)_x$ and $Ag^+(CO)_x$ complexes show similar patterns to that for $Cu^+(H_2O)_x$, but the bond energies to Ag^+ are much weaker (60% for $x = 1$ and 2 and 80% for $x = 3$ and 4 of the values for Cu^+) [67]. This is partly because the ionic radius of Ag^+ is larger (1.13 Å [82]), but for $x = 1$ and 2, this is primarily a result of the different energetic requirements for sd hybridization. Specifically, this hybridization involves interaction of the $^1S(s^0d^{10})$ and $^1D(s^1d^9)$ states. The latter is 315 kJ mol^{-1} above the ground state for Cu^+ and 551 kJ mol^{-1} high for Ag^+. A similar comparison between the bond energies of $Ni^+(CO)_x$, which are similar to those shown for $Ni^+(H_2O)_x$, and $Pt^+(CO)_x$ shows the latter are stronger [69]. This is counterintuitive because the promotion energy between the $^2D(s^0d^9)$ ground state and $^2F(s^1d^8)$ excited state is 162 kJ mol^{-1} for Ni^+ and 204 kJ mol^{-1} for Pt^+ [52] and the ionic radius of Pt^+ is larger than Ni^+ as well [82]. This difference is attributed to the relativistic effects and the lanthanide contraction, which make the 6s and 5d orbitals similar in size, allowing sd hybridization to be more efficient. In addition, as spin is no longer a very good quantum number for the third row metals, promotion to the $^4F(6s^15d^8)$ state at 73 kJ mol^{-1} is likely to be the appropriate energy to consider for Pt^+.

Although sequential bond energies of the late transition metals generally show the pattern exhibited in Fig. 3, other metals show much more distinctive patterns. Many of these have been discussed previously [4,26,60,80,81], but an illustrative example is that of Mn^+, shown in Fig. 4. Note that the three ligands shown all exhibit different patterns in the sequential bond energies. Our explanation for these differences can be understood by starting with the water complexes and comparing to values shown for Mg^+ [29], Fig. 4. The $Mg^+(H_2O)_x$ bond energies decline monotonically, indicating a largely electrostatic interaction, although this pattern hides the fact that Mg^+ (^2S, $3s^1$) utilizes sp hybridization to increase the strength of the bonding [86–88]. This is most evident in the geometry of the bis-ligated complexes [86,88], where the angle between ligands is much smaller than 180° because the ligands are repelled by the hybridized valence electron. Mn^+ (^7S, $4s^13d^5$) has a similar valence electron configuration as Mg^+, thus the first two bonds to water are quite similar in energy (and calculations indicate that $Mn^+(H_2O)_2$ also has a bent geometry [83,84]). For $M^+(H_2O)_3$, however, clearly something different happens for the two metals. The way to rationalize an increase in bonding is to move an electron from an antibonding orbital to a bonding or nonbonding orbital upon addition of another ligand. This is not possible for Mg^+, but for Mn^+, the repulsive interactions between the occupied 4s orbital and the ligands is removed in the $Mn^+(H_2O)_3$ complex by promoting the ion to the $^5D(4s^03d^6)$ state, which requires 174 kJ mol^{-1} [52]. Fewer ligands do not impose a

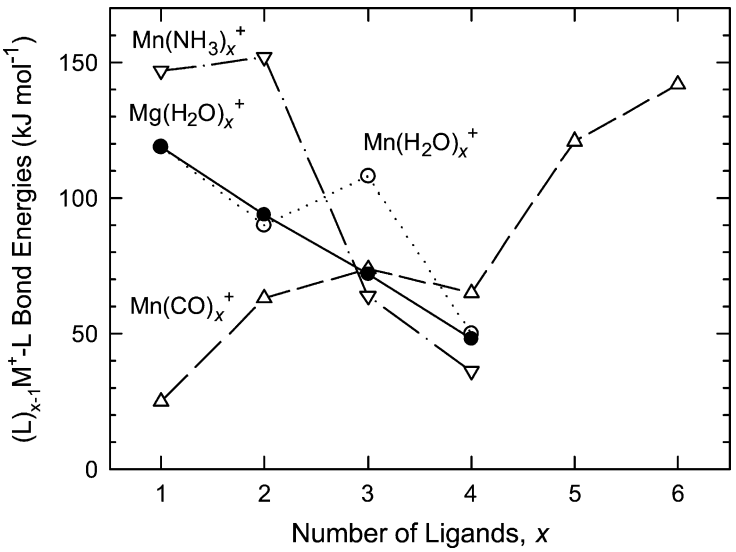

Fig. 4. Sequential bond energies (in kJ mol^{-1}) for water bound to Mg^+ (closed circles) and Mn^+ (open circles), ammonia bound to Mn^+ (open inverted triangles), and carbon monoxide bound to Mn^+ (open triangles).

strong enough ligand field to make the promotion and spin change energetically favorable. In contrast, the analogous increase in bond energies occurs after only two ammonia ligands, consistent with the stronger bonds formed by this ligand. The third and fourth ammonia ligands bind much more weakly because the sd hybridization effective for interaction with $Mn^+(^5D)$ is lost for more than two ligands, as argued above for Cu^+. The carbonyl bond energies exhibit an even more distinct trend. Again the $Mn^+(CO)$ bond energy is weak because of the repulsive interaction between the ligand and the occupied 4s orbital, however, unlike the polar water and ammonia molecules, CO cannot induce sp hybridization to strengthen this first bond. However, the ligand is a strong field ligand such that two COs are sufficient to induce the spin change to the quintet state [89], thereby increasing the bond energy for the second ligand. As additional ligands are added, the spin eventually changes to a singlet for $Mn^+(CO)_6$, an octahedral 18-electron complex [90]. Although the numbers of CO ligands required to induce the changes to triplet and then singlet states are not definitively known, these spin changes can explain the increase in bond energy observed for the more saturated complexes because in each case, electrons are moved from increasingly antibonding orbitals to nonbonding orbitals.

7. Metal cluster ligand bond energies

In addition to the bond energies of various ligands bound to single metal centers, the techniques elucidated above are applicable to the thermochemistry of metal cluster–ligand bonds. Thus, in reactions (1)–(3), the reactant M^+ is replaced with $M_m{}^+$. We have determined metal–metal bonds of such metal clusters using CID methods [4,91,92], and more recently measured the bond energies of various ligands to metal cluster cations [93,94]. These ligands include deuterium and oxygen atoms bound to vanadium [95,96], chromium [97–99], iron [100–102], and nickel [103] cluster cations. For iron clusters, we have also measured the binding energy of CD_x ligands where $x = 1$–3 [104]. Guided ion beam methods have also been used to quantitatively study the binding of carbonyls to metal cluster anions [105].

Values for all ligands measured with iron cluster cations are shown in Fig. 5. Several interesting trends are readily observed. There are substantial fluctuations

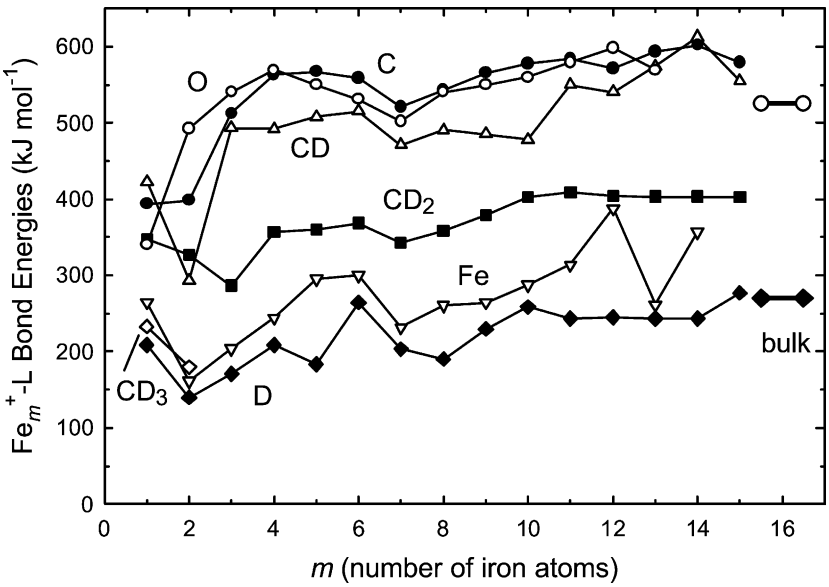

Fig. 5. Bond energies (in kJ mol^{-1}) for several ligands bound to iron clusters as a function of cluster size. Values shown for binding O and D to bulk iron surfaces are taken from [106–111]. Ligands include oxygen atoms (open circles), carbon atoms (closed circles), CD (open triangles), CD_2 (closed squares), iron atoms (open inverted triangles), CD_3 (open diamonds), and deuterium atoms (closed diamonds).

in the bond energies for small cluster sizes, consistent with strong variations in electronic and geometric structures. For larger clusters, the bond energies for each ligand reach values that do not change appreciably with cluster size. This asymptotic behavior occurs for clusters larger than about 10 atoms for most ligands, although the most strongly bound ligands can reach nearly constant cluster–ligand bond energies for much smaller clusters (down to about three atoms). In the two cases where values are available for binding to the bulk phase, (L = D and O [106–111]), the bond energies for large clusters are comparable to the bulk phase values. This suggests that chemical bonding is largely a local phenomenon and that modest sized clusters have enough electronic "flexibility" to form strong bonds with the ligands. This limit is reached at smaller cluster sizes for ligands that bind very strongly because they are able to disrupt the metal–metal bonding to their advantage. Finally, it is clear that the relative bond energies track nicely for species that form one (D and CD_3), two (CD_2), and three (CD) bonds to the metal clusters. These comparisons also suggest that surface oxides and carbides form three bonds to the surface, indicating that the two covalent bonds that these atoms can form are augmented by dative interactions, just as they were for single metal systems as discussed above. Note that because there is no literature information available for ligands that are molecular fragments (CD_x), the cluster ligand bond energies measured here provide some of the first experimental data available for such surface species.

Acknowledgements

I thank my students, listed in the references throughout this work, for their excellent work and insight. This work is supported by the National Science Foundation, Grant No. CHE-0135517.

References

[1] P.B. Armentrout, D.E. Clemmer, in: J.A.M. Simoes (Ed.), Energetics of Organometallic Species, Kluwer, Dordrecht, 1992, p. 321.
[2] P.B. Armentrout, in: D.H. Russell (Ed.), Gas Phase Inorganic Chemistry, Plenum Press, New York, 1989, p. 1.

[3] P.B. Armentrout, in: J.A. Davies, P.L. Watson, J.F. Liebman, A. Greenberg (Eds.), Selective Hydrocarbon Activation: Principles and Progress, VCH, New York, 1990, p. 467.
[4] P.B. Armentrout, B.L. Kickel, in: B.S. Freiser (Ed.), Organometallic Ion Chemistry, Kluwer, Dordrecht, 1996, p. 1.
[5] B.S. Freiser (Ed.), Organometallic Ion Chemistry, Kluwer, Dordrecht, 1996.
[6] P.B. Armentrout, in: J.M. Brown, P. Hofmann (Eds.), Topics in Organometallic Chemistry, vol. 4, Springer-Verlag, Berlin, 1999, p. 1.
[7] N. Aristov, P.B. Armentrout, J. Phys. Chem. 90 (1986) 5135.
[8] S.K. Loh, D.A. Hales, L. Lian, P.B. Armentrout, J. Chem. Phys. 90 (1989) 5466.
[9] D.A. Hales, P.B. Armentrout, J. Cluster Sci. 1 (1990) 127.
[10] K.M. Ervin, P.B. Armentrout, J. Chem. Phys. 83 (1985) 166.
[11] F. Muntean, P.B. Armentrout, J. Chem. Phys. 115 (2001) 1213.
[12] E. Teloy, D. Gerlich, Chem. Phys. 4 (1974) 417.
[13] D. Gerlich, in: C.-Y. Ng, M. Baer (Eds.), State-Selected and State-to-State Ion-Molecule Reaction Dynamics. Part 1: Experiment, Wiley, New York, 1992, p. 1.
[14] N. Aristov, P.B. Armentrout, J. Am. Chem. Soc. 108 (1986) 1806.
[15] W.J. Chesnavich, M.T. Bowers, J. Phys. Chem. 83 (1979) 900.
[16] P.B. Armentrout, J.L. Beauchamp, J. Chem. Phys. 74 (1981) 2819.
[17] J.L. Elkind, P.B. Armentrout, J. Phys. Chem. 88 (1984) 5454.
[18] M.E. Weber, J.L. Elkind, P.B. Armentrout, J. Chem. Phys. 84 (1986) 1521.
[19] K.M. Ervin, P.B. Armentrout, J. Chem. Phys. 86 (1987) 2659.
[20] B.H. Boo, P.B. Armentrout, J. Am. Chem. Soc. 109 (1987) 3549.
[21] L.S. Sunderlin, N. Aristov, P.B. Armentrout, J. Am. Chem. Soc. 109 (1987) 78.
[22] P.B. Armentrout, in: N.G. Adams, L.M. Babcock (Eds.), Advances in Gas Phase Ion Chemistry, vol. 1, JAI, Greenwich, 1992, p. 83.
[23] P.J. Chantry, J. Chem. Phys. 55 (1971) 2746.
[24] C. Lifshitz, R.L.C. Wu, T.O. Tiernan, D.T. Terwilliger, J. Chem. Phys. 68 (1978) 247.
[25] V.L. Talrose, P.S. Vinogradov, I.K. Larin, in: M.T. Bowers (Ed.), Gas Phase Ion Chemistry, vol. 1, Academic Press, New York, 1979, p. 305.
[26] N.F. Dalleska, K. Honma, P.B. Armentrout, J. Am. Chem. Soc. 115 (1993) 12125.
[27] R. Georgiadis, P.B. Armentrout, J. Am. Chem. Soc. 108 (1986) 2119.
[28] K.M. Ervin, P.B. Armentrout, J. Chem. Phys. 84 (1986) 6738.
[29] N.F. Dalleska, B.L. Tjelta, P.B. Armentrout, J. Phys. Chem. 98 (1994) 4191.
[30] M.T. Rodgers, P.B. Armentrout, J. Phys. Chem. A 101 (1997) 1238.
[31] P.B. Armentrout, L.F. Halle, J.L. Beauchamp, J. Chem. Phys. 76 (1982) 2449.
[32] P.A.M. van Koppen, J. Brodbelt-Lustig, M.T. Bowers, D.V. Dearden, J.L. Beauchamp, E.R. Fisher, P.B. Armentrout, J. Am. Chem. Soc. 112 (1990) 5663.
[33] P.A.M. van Koppen, J. Brodbelt-Lustig, M.T. Bowers, D.V. Dearden, J.L. Beauchamp, E.R. Fisher, P.B. Armentrout, J. Am. Chem. Soc. 113 (1991) 2359.
[34] C.L. Haynes, Y.M. Chen, P.B. Armentrout, J. Phys. Chem. 99 (1995) 9110.
[35] C.L. Haynes, Y.M. Chen, P.B. Armentrout, J. Phys. Chem. 100 (1996) 111.
[36] P.B. Armentrout, J. Simons, J. Am. Chem. Soc. 114 (1992) 8627.
[37] R.H. Schultz, K.C. Crellin, P.B. Armentrout, J. Am. Chem. Soc. 113 (1991) 8590.
[38] D.A. Hales, L. Lian, P.B. Armentrout, Int. J. Mass. Spectrom. Ion Processes 102 (1990) 269.
[39] P.J. Robinson, K.A. Holbrook, Unimolecular Reactions, Wiley, London, 1972.
[40] F.A. Khan, D.E. Clemmer, R.H. Schultz, P.B. Armentrout, J. Phys. Chem. 97 (1993) 7978.
[41] M.T. Rodgers, K.M. Ervin, P.B. Armentrout, J. Chem. Phys. 106 (1998) 4499.
[42] F. Muntean, L. Heumann, P.B. Armentrout, J. Chem. Phys. 116 (2002) 5593.
[43] F. Muntean, P.B. Armentrout, J. Phys. Chem. B 106 (2002) 8117.
[44] I. Kretzschmar, D. Schröder, H. Schwarz, P.B. Armentrout, in: M.A. Duncan (Ed.), Advances in Metal and Semiconductor Clusters, vol. 5, 2001, p. 347.
[45] N. Aristov, P.B. Armentrout, J. Am. Chem. Soc. 106 (1984) 4065.
[46] Y.-M. Chen, M.R. Sievers, P.B. Armentrout, Int. J. Mass Spectrom. Ion Processes 167/168 (1997) 195.
[47] Y.-M. Chen, P.B. Armentrout, J. Chem. Phys. 103 (1995) 618.
[48] Y.-M. Chen, J.L. Elkind, P.B. Armentrout, J. Phys. Chem. 99 (1995) 10438.
[49] X.-G. Zhang, R. Liyanage, P.B. Armentrout, J. Am. Chem. Soc. 123 (2001) 5563.
[50] X.-G. Zhang, P.B. Armentrout, J. Chem. Phys. 116 (2002) 5565.
[51] X.-G. Zhang, P.B. Armentrout, J. Phys. Chem. A, submitted for publication.
[52] C.E. Moore, Atomic Energy Levels, NSRDS-NBS 35 (1971) vols. I–III.
[53] K.K. Irikura, J.L. Beauchamp, J. Phys. Chem. 95 (1991) 8344.
[54] K.K. Irikura, W.A. Goddard III, J. Am. Chem. Soc. 116 (1994) 8733.
[55] E.R. Fisher, J.L. Elkind, D.E. Clemmer, R. Georgiadis, S.K. Loh, N. Aristov, L.S. Sunderlin, P.B. Armentrout, J. Chem. Phys. 93 (1990) 2676.
[56] N.F. Dalleska, K. Honma, L.S. Sunderlin, P.B. Armentrout, J. Am. Chem. Soc. 116 (1994) 3519.
[57] P.B. Armentrout, ACS Symp. Ser. 428 (1990) 18.

[58] P.B. Armentrout, R. Georgiadis, Polyhedron 7 (1988) 1573.
[59] J.L. Tilson, J.F. Harrison, J. Phys. Chem. 95 (1991) 5097.
[60] D. Walter, P.B. Armentrout, J. Am. Chem. Soc. 120 (1998) 3176.
[61] M.T. Rodgers, J.R. Stanley, R. Amunugama, J. Am. Chem. Soc. 122 (2000) 10969.
[62] R. Amunugama, M.T. Rodgers, J. Phys. Chem. A 105 (2001) 9883.
[63] M.T. Rodgers, P.B. Armentrout, J. Am. Chem. Soc. 124 (2002) 2678.
[64] S. Goebel, C.L. Haynes, F.A. Khan, P.B. Armentrout, J. Am. Chem. Soc. 117 (1995) 6994.
[65] M.R. Sievers, P.B. Armentrout, J. Phys. Chem. 99 (1995) 8135.
[66] F.A. Khan, D.L. Steele, P.B. Armentrout, J. Phys. Chem. 99 (1995) 7819.
[67] F. Meyer, Y.M. Chen, P.B. Armentrout, J. Am. Chem. Soc. 117 (1995) 4071.
[68] F. Meyer, P.B. Armentrout, Mol. Phys. 88 (1996) 187.
[69] X.-G. Zhang, P.B. Armentrout, Organometallics 20 (2001) 4266.
[70] M.R. Sievers, L.M. Jarvis, P.B. Armentrout, J. Am. Chem. Soc. 120 (1998) 1891.
[71] F. Meyer, F.A. Khan, P.B. Armentrout, J. Am. Chem. Soc. 117 (1995) 9740.
[72] B.L. Tjelta, P.B. Armentrout, J. Phys. Chem. A 101 (1997) 2064.
[73] K. Koszinowski, D. Schröder, H. Schwarz, M.C. Holthausen, J. Sauer, H. Koizumi, P.B. Armentrout, Inorg. Chem. 41 (2002) 5882, 7170.
[74] C.L. Haynes, P.B. Armentrout, J.K. Perry, W.A. Goddard, J. Phys. Chem. 99 (1995) 6340.
[75] R.H. Schultz, P.B. Armentrout, J. Phys. Chem. 97 (1993) 596.
[76] G. Vitale, A.B. Valina, H. Huang, R. Amunugama, M.T. Rodgers, J. Phys. Chem. A 105 (2001) 11351.
[77] Y. Chu, Z. Yang, M.T. Rodgers, J. Am. Soc. Mass Spectrom. 13 (2002) 453.
[78] H. Koizumi, X.-G. Zhang, P.B. Armentrout, J. Phys. Chem. A 105 (2001) 2444.
[79] H. Koizumi, P.B. Armentrout, J. Am. Soc. Mass Spectrom. 12 (2001) 480.
[80] P.B. Armentrout, Acc. Chem. Res. 28 (1995) 430.
[81] M. T Rodgers, P.B. Armentrout, Mass Spectrom. Rev. 19 (2000) 215.
[82] R.G. Wilson, G.R. Brewer, Ion Beams, Wiley, New York, 1973.
[83] M. Rosi, C.W. Bauschlicher, J. Chem. Phys. 90 (1989) 7264.
[84] M. Rosi, C.W. Bauschlicher, J. Chem. Phys. 92 (1990) 1876.
[85] C.W. Bauschlicher, S.R. Langhoff, H. Partridge, in: B.S. Freiser (Ed.), Organometallic Ion Chemistry, Dordrecht, Kluwer, 1996, p. 47.
[86] C.W. Bauschlicher, H. Partridge, J. Phys. Chem. 95 (1991) 9694.
[87] C.W. Bauschlicher, M. Sodupe, H. Partridge, J. Chem. Phys. 96 (1992) 4453.
[88] A. Andersen, F. Muntean, D. Walter, C. Rue, P.B. Armentrout, J. Phys. Chem. A 104 (2000) 692.
[89] L.A. Barnes, M. Rosi, C.W. Bauschlicher, J. Chem. Phys. 93 (1990) 609.
[90] N.A. Beach, H.B. Gray, J. Am. Chem. Soc. 90 (1968) 5713.
[91] P.B. Armentrout, D.A. Hales, L. Lian, in: M.A. Duncan (Ed.), Advances in Metal and Semiconductor Clusters, vol. 2, JAI, Greenwich, 1994, p. 1.
[92] P.B. Armentrout, in: N. Russo, D.R. Salahub (Eds.), Metal–Ligand Interactions—Structure and Reactivity, Kluwer, Dordrecht, 1996, p. 23.
[93] P.B. Armentrout, J.B. Griffin, J. Conceição, in: G.N. Chuev, V.D. Lakhno, A.P. Nefedov (Eds.), Progress in Physics of Clusters, World Scientific, Singapore, 1999, p. 198.
[94] P.B. Armentrout, Ann. Rev. Phys. Chem. 52 (2001) 423.
[95] J. Xu, M.T. Rodgers, J.B. Griffin, P.B. Armentrout, J. Chem. Phys. 108 (1998) 9339.
[96] R. Liyanage, J. Conceição, P.B. Armentrout, J. Chem. Phys. 116 (2002) 936.
[97] J.B. Griffin, P.B. Armentrout, J. Chem. Phys. 108 (1998) 8062.
[98] J.B. Griffin, P.B. Armentrout, J. Chem. Phys. 108 (1998) 8075.
[99] J. Conceição, R. Liyanage, P.B. Armentrout, Chem. Phys. 262 (2000) 115.
[100] J. Conceição, S.K. Loh, L. Lian, P.B. Armentrout, J. Chem. Phys. 104 (1996) 3976.
[101] J.B. Griffin, P.B. Armentrout, J. Chem. Phys. 106 (1997) 4448.
[102] J.B. Griffin, P.B. Armentrout, J. Chem. Phys. 107 (1997) 5345.
[103] F. Liu, R. Liyanage, P.B. Armentrout, J. Chem. Phys. 117 (2002) 132.
[104] R. Liyanage, X.-G. Zhang, P.B. Armentrout, J. Chem. Phys. 115 (2001) 9747.
[105] K.M. Ervin, Int. Rev. Phys. Chem. 20 (2001) 127.
[106] F. Boszo, G. Ertl, M. Grunze, M. Weiss, Appl. Surf. Sci. 1 (1977) 103.
[107] F. Boszo, G. Ertl, M. Weiss, J. Catal. 50 (1977) 519.
[108] J.B. Benziger, in: E. Shustorovich (Ed.), Metal–Surface Reaction Energetics, VCH, New York, 1991, p. 53.
[109] D. Brennan, D.O. Hayward, B.M.W. Tradnell, Proc. Roy. Soc. A256 (1960) 81.
[110] J. Bragg, F.C. Tomkins, Trans. Faraday Soc. 51 (1955) 1071.
[111] G. Wedler, Z. Phys. Chem. 27 (1961) 388.
[112] I. Kretzschmar, D. Schröder, H. Schwarz, C. Rue, P.B. Armentrout, J. Phys. Chem. A 104 (2000) 5046.
[113] I. Kretzschmar, D. Schröder, H. Schwarz, C. Rue, P.B. Armentrout, J. Phys. Chem. A 102 (1998) 10060.
[114] C. Rue, P.B. Armentrout, I. Kretzschmar, D. Schröder, H. Schwarz, Int. J. Mass Spectrom. 210/211 (2001) 283.
[115] R.L. Hettich, B.S. Freiser 108 (1986) 2537.
[116] D. Schröder, I. Kretzschmar, H. Schwarz, C. Rue, P.B. Armentrout, Inorg. Chem. 38 (1999) 3474.

[117] C. Rue, P.B. Armentrout, I. Kretzschmar, D. Schröder, H. Schwarz, J. Phys. Chem. A 105 (2001) 8456.
[118] C. Rue, P.B. Armentrout, I. Kretzschmar, D. Schröder, H. Schwarz, J. Phys. Chem. A 106 (2002) 9788.
[119] M.T. Rodgers, B. Walker, P.B. Armentrout, Int. J. Mass Spectrom. 182/183 (1999) 99.
[120] M.R. Sievers, Y.-M. Chen, J.L. Elkind, P.B. Armentrout, J. Phys. Chem. 100 (1996) 54.
[121] M.R. Sievers, Y.-M. Chen, P.B. Armentrout, J. Chem. Phys. 105 (1996) 6322.
[122] M.R. Sievers, Y.-M. Chen, C.L. Haynes, P.B. Armentrout, Int. J. Mass Spectrom. 195/196 (2000) 149.
[123] P.B. Armentrout, Y.-M. Chen, J. Am. Soc. Mass Spectrom. 10 (1999) 821.
[124] Y.-M. Chen, P.B. Armentrout, J. Am. Chem. Soc. 117 (1995) 9291.
[125] Y.-M. Chen, P.B. Armentrout, J. Phys. Chem. 99 (1995) 11424.
[126] X.-G. Zhang, C. Rue, S.-Y. Shin, P.B. Armentrout, J. Chem. Phys. 116 (2002) 5574.